01 Jan 1991

Decoupled Dynamics for Control and Estimation

S. N. Balakrishnan

Missouri University of Science and Technology, bala@mst.edu

DECOUPLED DYNAMICS FOR CONTROL AND ESTIMATION

S. N. Balakrishnan

University of Missouri-Rolla

Abstract

Decoupling of the dynamical equations in polar coordinates is used to develop a control scheme for use in target-intercept problems with passive measurements. By defining a pseudo control variable in the radial coordinate, the radial dynamics is made independent of the transverse dynamics. After solving for the radial control, the transverse control is determined through solutions to a two-point boundary value problem. Numerical experiments are presented with a six degrees of freedom simulation.

I. Introduction

Major difficulties in obtaining better performance with a modern control based homing guidance have been due to the nonlinearity of the dynamic/measurement process. In an inertial system either the dynamics and/or the measurements are always nonlinear. The most widely used method to solve the target-intercept problem has been the extended Kalman filter[1] with an 'optimal' linear guidance law[2] formulated in a set of rectangular Cartesian coordinates. The state space usually consists of the relative positions, relative velocities, and the target accelerations[3-5]. However, the importance and the advantages of a polar coordinate based formulation has been stressed in a few studies recently[4-7]. The existing studies[3-6] have been limited to the formulation of the filtering problem in the polar coordinates. In this study, however, solutions to the 'optimal' guidance problem has been attempted in polar coordinates. This paper has been organized as follows: the formulation and solutions of the optimal guidance problem in a set of polar coordinates is described in Section II. The system model and the measurement model are presented in Section III. The numerical experiments and the results are described in Section IV. Conclusions are summarized in Section V.

II. Optimal Guidance in Decoupled Polar Coordinates

The dynamics of the target-intercept problem is a coupled nonlinear problem in an inertial polar coordinate system. In a three dimensional geometry it is stated as

$$\ddot{R} - R\dot{\theta}^2 = a_{T_R} - a_{M_R} \qquad (1)$$

and

$$R\ddot{\theta} + 2\dot{R}\dot{\theta} = a_{T_\theta} - a_{M_\theta} \qquad (2)$$

$$\ddot{z} = a_{T_z} - a_{M_z} \qquad (3)$$

where R is the relative range between the target and the missile, θ is the bearing angle and a_{T_R} and a_{T_θ} are the target acceleration components in the line-of-sight and transverse directions, respectively. Similarly, a_{M_R} and a_{M_θ} are the missile commanded accelerations in the line-of-sight and the transverse directions, respectively. Dots denote differentiations with respect to time.

Radial (Line-of-sight) Acceleration

It can be observed that Equations (1) and (2) are coupled. In order to decouple the dynamics, a pseudo-control, $a_{M_{R_1}}$, is defined as

$$a_{M_{R_1}} = a_{M_R} - R\dot{\theta}^2 \qquad (4)$$

Note that this definition decouples the transverse coordinate from the radial coordinate. Now we can define a state space, y, in the line-of-sight direction as $y = [R, \dot{R}, a_{T_R}]^T$ and describe the dynamics as

$$\dot{y}_1 = y_2 \qquad (5a)$$

$$\dot{y}_2 = y_3 - a_{M_{R_1}} \qquad (5b)$$

CH3007-2/91/0000-1332 $1.00 © 1991 IEEE

$$\dot{y}_3 = -\lambda_R y_3 \qquad (5c)$$

λ_R is the time constant or the exponential correlation constant in a linear model.

The optimal guidance law in the radial direction is obtained as a solution to minimizing the performance index, J_1, where

$$J_1 = \frac{1}{2} S_{R_f} y_{1_f}^2 + \frac{1}{2} \int_0^{t_f} \gamma \, a_{M_{R1}}^2 \, dt \qquad (6)$$

where S_{R_f} is the weight on the terminal miss distance and γ is the weight on the control effort, and t_f is the time-to-go. The time-to-go, t_f, is approximated as $|R|/\dot{R}$ assuming constant relative velocity along the line-of-sight. The control, $a_{M_{R_1}}$, which minimizes Eq. (6) is given by

$$a_{M_{R_1}}(t) = \frac{t_f}{\gamma} \lambda_1 \text{ where} \qquad (7)$$

$$\lambda_1 = S_f(y_1 + t_f y_2 + \frac{1}{\lambda_R^2} a_{T_R} [\exp(-\lambda_R t_f) + \lambda_R t_f - 1]/ (1 + t_f^3 S_f/3\gamma) \qquad (8)$$

λ_1 is the Lagrangian multiplier which is used to adjoin Eqn. (5b) to the performance index in Eq. (6).

The commanded acceleration along the line-of-sight can be obtained as

$$a_{M_R}(t) = a_{M_{R_1}}(t) + R\dot{\theta}^2 \qquad (9)$$

Note that the relative range and the range rates can be obtained through integration of Eq. (5)

$$y_2(t) = y_{20} + (t^2 - 2t_f t)\lambda_R/2\gamma - y_{30}(\exp(-\lambda_R t)-1)/\lambda_R \qquad (10)$$

$$y_1(t) = y_{10} + t\, y_{20} + y_{30}(\exp(-\lambda_R t) + \lambda_R t - 1)/\lambda_R^2 + (t^3 - 3t_f t^2)\lambda_R/6\gamma \qquad (11)$$

Transverse Acceleration

The equation of motion in the transverse direction given by Eq. (2) can be rewritten as

$$\ddot{\theta} = -2\dot{R}\dot{\theta}/R + \frac{1}{R} a_{T_\theta} - \frac{1}{R} a_{M_\theta} \qquad (12)$$

Since R and $\dot{R}$ are known through Eq. (9) and (10) they can be treated as functions of time only. Consequently, Eq. (11) is expressed as

$$\ddot{\theta} = f(t)\dot{\theta} + g(t)a_{T_\theta} - g(t)a_{M_\theta} \qquad (13)$$

Where f(t) = -2R/R and g(t) = 1/R. By using a state space $z = [\theta, \dot{\theta}, a_{T_\theta}]^T$, Eq. (13) becomes

$$\dot{z}_1 = z_2 \qquad (13a)$$

$$\dot{z}_2 = f(t)z_2 + g(t)z_3 - g(t)a_{M_\theta} \qquad (13b)$$

$$\text{and } \dot{z}_3 = -\lambda_\theta z_3. \qquad (13c)$$

In Eq. (13c), λ_θ is the time constant. The transverse control acceleration, a_{M_θ} is found as a solution to the minimization of the cost function, J_1, where

$$J_1 = \frac{1}{2} S_{f_\theta} z_{2_f}^2 + \frac{1}{2} \int_0^{t_f} (\gamma_1 z_2^2 + \gamma_2 a_{M^\theta}^2)\, dt \qquad (15)$$

where S_{f_θ}, γ_1, and γ_2 are the weights.

The line-of-sight rate, z_2, is kept small so as to help the intercept. The optimization process for J_1 results in a two-point boundary value problem. This is described by

$$\begin{bmatrix} \dot{z}_2 \\ \dot{\lambda}_2 \end{bmatrix} = \begin{bmatrix} f(t) & -g^2(t)/\gamma_2 \\ -\gamma_1 & -f(t) \end{bmatrix}$$

$$\begin{bmatrix} z_2 \\ \lambda_2 \end{bmatrix} + \begin{bmatrix} g(t)\ z_{30}\exp(-\lambda_\theta t) \\ 0 \end{bmatrix} \tag{16}$$

with z_{20} known and $\lambda_f = S_{f_\theta}\, z_{2f}$. In Eq. (15) λ_2 represents the Lagrangian multiplier which is used to adjoin Eq. (13b) to the performance index, J_1. This system is solved by using a shooting method[1]. The transverse control can be calculated from the optimality condition as

$$a_{M_\theta}(t) = \lambda_2 g(t)/\gamma_2 \tag{17}$$

Vertical Acceleration

The commanded acceleration in the vertical direction is obtained in exactly the same manner as the radial acceleration.

III. System and Measurement Model

For the simulations, the system and the measurement models have been formulated in an inertial Cartesian frame so as to obtain closed form solutions between the measurement updates.

The target and the observer are represented as point masses in the tracking simulation. The target is assumed to move with a constant velocity. However, in the filtering process, its acceleration has been modeled as a stochastic process to reflect the observer's lack of knowledge about the target motion. The system model is given by

$$\dot{x}(t) = Fx(t) + b(t) + w(t) \tag{18}$$

where $x = [x_R, y_R, z_R, \dot{x}_R, \dot{y}_R, \dot{z}_R, a_{T_x}, a_{T_y}, a_{T_z}]^T$, with the first three variables representing the relative positions, the second three representing the relative velocities, and the last three denoting the target accelerations along x, y and z axes, respectively.

$$F = \begin{bmatrix} 0 & I & 0 \\ 0 & 0 & I \\ 0 & 0 & \lambda_T \end{bmatrix} \tag{19}$$

with each partition representing a 3x3 matrix. The quantity λ_T is given by

$$\lambda_T = \begin{bmatrix} \lambda_t & 0 & 0 \\ 0 & \lambda_t & 0 \\ 0 & 0 & \lambda_t \end{bmatrix} \tag{20}$$

Note that when λ_t is zero, the target motion is a Brownian motion process. The nine-element vector b is given by

$$b = [0,0,0,a_{M_x},\ a_{M_y},a_{M_z},0,0,0]^T \tag{21}$$

where a_{M_x}, a_{M_y}, a_{M_z} are the components of the observer acceleration in the x, y, and z directions, respectively. The nine-element noise vector w has only three nonzero components w_{T_x}, w_{T_y}, and w_{T_z} in the target acceleration dynamics in the x, y, and z directions, respectively.

The measurement model shown in Figure (1) is given by

$$z_{1i} = \tan^{-1}(y_{R_i}/x_{R_i}) + v_{1i} \tag{22a}$$

$$z_{2i} = \tan^{-1}(-z_{R_i}/\sqrt{x_{R_i}^2 + y_{R_i}^2}) + v_{2i} \tag{22b}$$

where z_{1i} and z_{2i} are the discrete measurement at stage i and x_{R_i}, y_{R_i}, and z_{R_i} are the corresponding relative positions. The noises v_{1i} and v_{2i} are white, random sequences, with mean zero and variance V.

Because of the linearity of Eq. (18), the mean states can be propagated in a closed form as

$$x(t) = \phi(t,t_0)x_0 + \int_{t_0}^{t} \phi(t,\tau)b(\tau)d\tau \tag{23}$$

where

$$\phi(t,\tau) = \begin{bmatrix} 1 & 0 & 0 & \alpha & 0 & 0 & \Delta_1 & 0 & 0 \\ 0 & 1 & 0 & 0 & \alpha & 0 & 0 & \Delta_1 & 0 \\ 0 & 0 & 1 & 0 & 0 & \alpha & 0 & 0 & \Delta_1 \\ 0 & 0 & 0 & 1 & 0 & 0 & \Delta_2 & 0 & 0 \\ 0 & 0 & 0 & 0 & 1 & 0 & 0 & \Delta_2 & 0 \\ 0 & 0 & 0 & 0 & 0 & 1 & 0 & 0 & \Delta_2 \\ 0 & 0 & 0 & 0 & 0 & 0 & \Delta_3 & 0 & 0 \\ 0 & 0 & 0 & 0 & 0 & 0 & 0 & \Delta_3 & 0 \\ 0 & 0 & 0 & 0 & 0 & 0 & 0 & 0 & \Delta_3 \end{bmatrix} \tag{24}$$

$$\alpha = t-\tau$$

$$\Delta_1 = \frac{1}{\lambda_t^2}\left(\exp[-\lambda_t(t-\tau)]+\lambda_t(t-\tau)-1\right.$$

$$\Delta_2 = -\frac{1}{\lambda_t}[\exp(-\lambda_t(t-\tau))-1]$$

$$\Delta_3 = \exp[-\lambda_t(t-\tau)]$$

IV. Numerical Results

A six degree-of-freedom computer program which simulates the interception of a maneuvering target by a bank-to-turn, short-range, air-to-air homing missile has been used to test the control scheme developed in Section II. The launch geometry used in this analysis is described in Figure 2. For this inertial system, the z_I axis is directed towards the earth's center, the x_I axis is aligned parallel with the missile's initial launch direction, and the y_I axis is chosen to make the inertial system right handed. The engagement geometry is characterized by the initial conditions: range, 3000 feet; altitude, 10,000 feet; aspect angle (θ_a), and off-boresight angle (θ_b). The states of the filter on board the missile are the positions and velocities with respect to the target and the target acceleration. In the simulation, the target initiates a nine-g maneuver 45° up and to the right relative to its reference frame. This maneuver continues till the time-to-go, defined as the ratio of the relative range to range rate reaches one second. At this epoch, the target rolls 180° and pulls 9-g's till the engagement is concluded. However, in the filters, the target acceleration is modeled as a first-order Markov process.

The diagonal elements of the initial state covariance are 10^7 ft^2 for the relative positions, 100 ft^2/sec^2 for the relative velocities, and 10 ft^2/sec^4 for the target accelerations. The off-diagonal elements are zero. The power spectral density of the process noise is 50000 ft^2/sec^3 in all the directions. In all cases, the initial range between the target and the missile is 3000 ft.

In this study, two types of comparative analyses are made. In the first case, deterministic models of the engagement are used and the present scheme is compared with the linear optimal guidance law[2] which uses an inertial rectangular coordinate frame. The second type deals with the stochastic case where the inputs to the guidance law, namely, the states of the system are provided through an extended Kalman filter[2] with the system model as described in Section III.

Representative results of both cases are provided in Table I and Figures 3-12.

It can be seen from Table I that the results using the decoupled polar control (DPC) results in smaller miss distances as compared to the Cartesian based control (CBC). The advantage of using the decoupled control becomes clearer in scenarios where the missile has to make a tighter turn as when the initial off-boresight angle is 40° and the aspect angle is 120°. With the DPC, in the transverse coordinates, the designer is able to exercise control on the line-of-sight rate (within the autopilot limits) through the weight in the cost function and therefore, able to control the relative geometry better than in the case of a CBC.

The engagement histories of the DPC and the CBC for an initial range of 3000 ft, aspect angle, 120°, and off-boresight angle of 40° are presented in Figures 3 and 4, and 5 and 6, respectively. While the CBC based missile misses the target totally (the range rate becomes positive) at 1.32 seconds, the DPC based missile is able to capture the target with a miss distance of 2 ft.

The results of the stochastic cases are presented in Figures 7 through 12. The error histories in the magnitudes of range, range rate, and the target acceleration for boresight angles of 60° and 120° are presented in Figures 7-9 and 10-12, respectively. The initial peak values in the range errors are due to the high values of the state covariance matrix elements which are 10^7 ft^2/sec^2. The errors diminish when information becomes available. After the second target maneuver of nine g's takes place, the correlations of errors are no longer valid and therefore, the error histories again show increases. However, they show decreasing trend again since the closing geometry is highly observable. The spikes in the values of the errors at the end of the geometry are due to the observation residuals at the end of the engagement and are not meaningful to the working of the filter or the control.

V. Conclusions

An optimal control law based on the decoupling of a set of polar coordinates has been developed in this paper. Numerical results from a six degree-of-freedom simulations which use the decoupled control indicate

that it is better than the completely Cartesian coordinate control for most of the cases. The decoupled control, though, is obtained iteratively through a two-point boundary value problem and hence, is more computationally intensive. The extension of this work to the filters is under way.

References

1. Bryson, A. E. and Ho, Y. C., Applied Optimal Control, Waltham, Mass., Blaisdell, 1969.

2. Fiske, P. H., "Advanced Digital Guidance and Control Concepts for Air-to-Air Tactical Missiles," Final Report, AFATL-TR-77-130, November 1977.

3. Sammons, J. M., Balakrishnan, S. N., Speyer, J. L., Hull, D. G., "Development and Comparison of Optimal Filters," Final Report, AFATL-TR-79-87, October 1979.

4. Balakrishnan, S. N. and Speyer, J. L., "A Coordinate Transformation Based on Filter for Improved Target Tracking," Journal of Guidance, Dynamics, and Control, November-December 1986.

5. Balakrishnan, S. N. and Speyer, J. L., "Assumed Density Filter with Application to Homing Missile Guidance," Journal of Guidance, Control, and Dynamics, January-February 1989.

6. Balakrishnan, S. N., "Observability Results and Improved Performance with a Tracking Filter Using Passive Measurements," Journal of Guidance, Control, and Dynamics, January-February 1990.

7. Cloutier, J. R., Evers, J. H., and Feely, J. J., "An Assessment of Air-to-Air Missile Guidance and Control Technology," 1988 American Control Conference, Atlanta, GA, June 1988, pp. 133-142.

Table I

Launch Range = 3000 ft.

Engagement No.	Off Boresight Angle	Aspect Angle	Miss Dist. (ft) DPC	CBC
1	0	60°	2.5	1.3
2	0	120°	13	17
5	40°	120°	2	1866
6	40°	150°	662	731
7	40°	180°	243	259
3	0	150°	26	8 ft
4	0	180°	2	1 ft

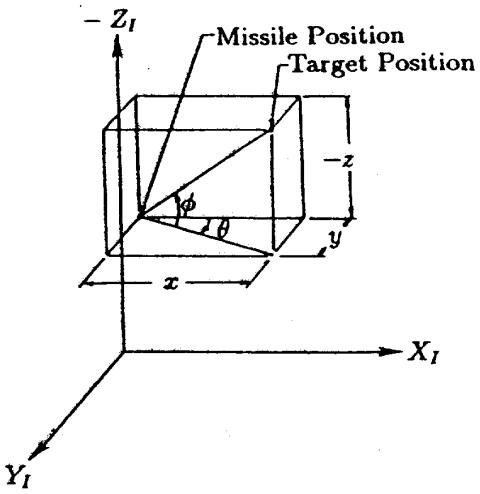

Figure 1. Intercept Geometry and Measurement Angles.

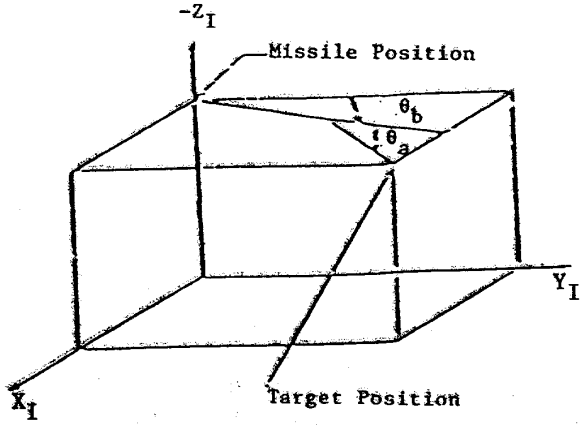

Figure 2. Launch Geometry.

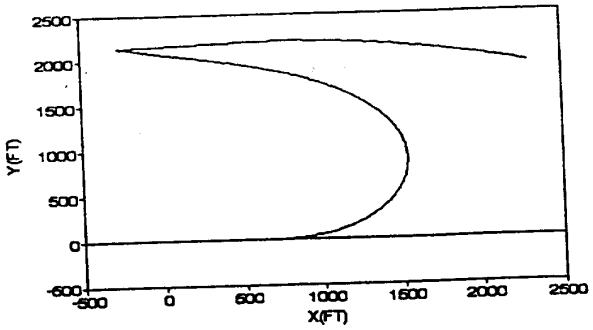

Figure 3. DPC Used Trajectories in x-y Plane.

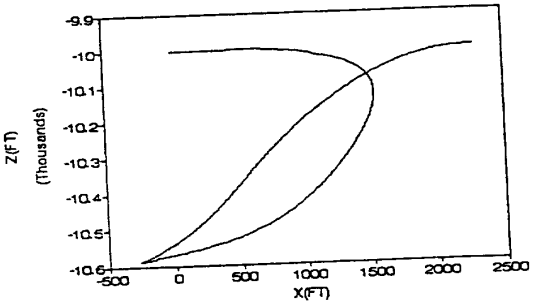

Figure 4. DPC Used Trajectories in x-z Plane.

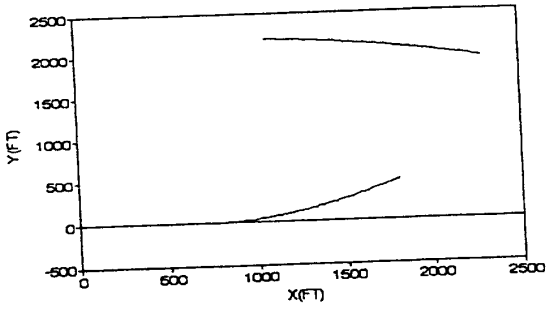

Figure 5. CBC Used Trajectories in x-y Plane.

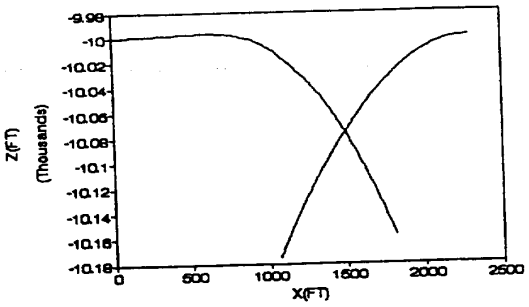

Figure 6. CBC Used Trajectories in x-z Plane.

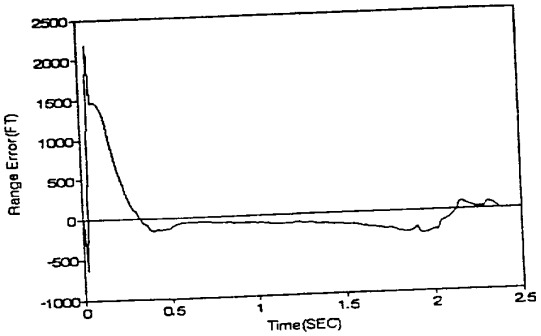

Figure 7. Range Error History, R = 3000 ft, $\theta_a = 60°, \theta_b = 0°$.

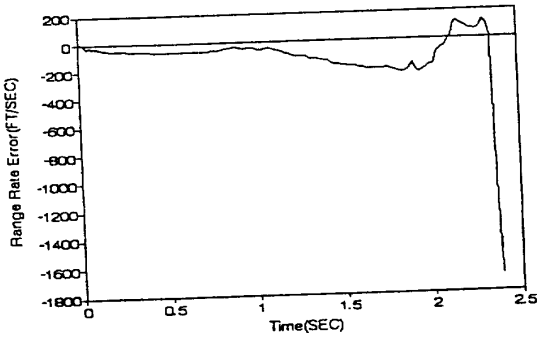

Figure 8. Range Rate Error History, R = 3000 ft, $\theta_a = 60°, \theta_b = 0°$.

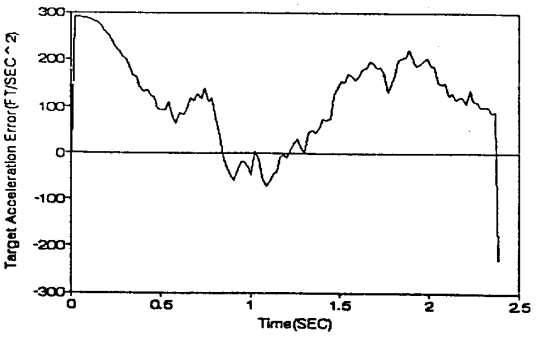

Figure 9. Target Acceleration Error History, R = 3000 ft, $\theta_a = 60°$, $\theta_b = 0°$.

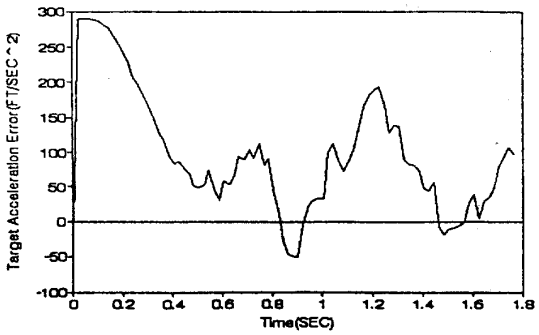

Figure 12. Target Acceleration Error History, R = 3000 ft, $\theta_a = 60°$, $\theta_b = 0°$.

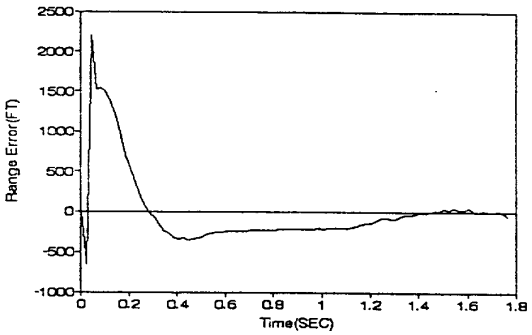

Figure 10. Range Error History, R = 3000 ft, $\theta_a = 60°$, $\theta_b = 0°$.

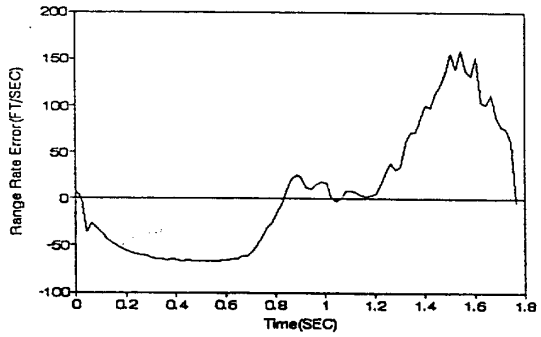

Figure 11. Range Rate Error History, R = 3000 ft, $\theta_a = 60°$, $\theta_b = 0°$.